

High-Throughput Nanofabrication of Infrared Plasmonic Nanoantenna Arrays for Vibrational Nanospectroscopy

Serap Aksu,^{†,‡} Ahmet A. Yanik,^{‡,§} Ronen Adato,^{‡,§} Alp Artar,^{‡,§} Min Huang,^{‡,§} and Hatice Altug^{*,†,‡,§}

[†]Materials Science and Engineering, [‡]Photonics Center, and [§]Electrical and Computer Engineering, Boston University, Boston, Massachusetts 02215

ABSTRACT The introduction of high-throughput and high-resolution nanofabrication techniques operating at low cost and low complexity is essential for the advancement of nanoplasmonic and nanophotonic fields. In this paper, we demonstrate a novel fabrication approach based on nanostencil lithography for high-throughput fabrication of engineered infrared plasmonic nanorod antenna arrays. The technique relying on deposition of materials through a shadow mask enables plasmonic substrates supporting spectrally sharp collective resonances. We show that reflectance spectra of these antenna arrays are comparable to that of arrays fabricated by electron beam lithography. We also show that nanostencils can be reused multiple times to fabricate a series of infrared nanoantenna arrays with identical optical responses. Finally, we demonstrate fabrication of plasmonic nanostructures in a variety of shapes with a single metal deposition step on different substrates, including nonconducting ones. Our approach, by enabling the reusability of the stencil and offering flexibility on the substrate choice and nanopattern design, could facilitate the transition of plasmonic technologies to the real-world applications.

KEYWORDS Shadow mask, nanostencil lithography, optical nanoantennas, surface plasmons, near-field enhancement, infrared spectroscopy

Nanoplasmonics, optical studies of tailored metallic nanostructures and their applications, has emerged as a rapidly growing field in recent years.^{1–3} By enabling subwavelength light localization and dramatically strong local fields, plasmonics is opening up a myriad of exciting possibilities.^{4–7} Plasmons have been used to enhance linear and nonlinear optical phenomena including fluorescence,^{8,9} surface enhanced spectroscopy^{10–14} and high-order harmonic generation.¹⁵ In a recent paper, we have shown that large field enhancements in plasmonics could lead to ultrasensitive infrared spectroscopy and enable detection of vibrational signatures of proteins at zepto-mole sensitivity levels.¹⁶ Proof of concept devices such as plasmon based sources,^{17–19} superlenses,^{20,21} and metamaterials^{22–24} have already been demonstrated. Furthermore, by enabling optical and electrical signal transmission through the same metal circuitry, plasmonics could also lead to large scale on-chip integration of electronic and photonic components.²⁵

Such advances in nanoplasmonics, however, are critically dependent on our ability to structure metals in a controllable way at sub-100 nm resolution. The most common top-down nanopatterning techniques with high resolution are electron beam²⁶ and focused ion beam²⁷ lithography. Electron beam lithography (EBL) is mostly used for on-chip plasmonic nanoparticle array fabrication, while focused ion beam (FIB)

tools are reserved primarily to fabricate nanoapertures in metallic films. Both EBL and FIB offer tremendous flexibility in creating large variety of nanostructure geometries and patterns at high resolution. However, their major drawback is the low-throughput. Each nanostructure is lithographically defined in a serial manner, which is both slow and expensive. In addition, for EBL the choice of substrates is also limited due to the dependence of the e-beam exposure on the substrate conductivity. For example, patterning on glass substrates could be done by adding a conductive film (such as ITO). But, this conductive layer could interfere with the optical responses of the fabricated nanostructures.²⁸ Plasmonic nanoparticle and nanowire fabrication with EBL often involves a lift-off process, which can be restrictive in creating nanostructures with high aspect ratios. Although, multilayer lithographic processes are offered to be solutions for this limitation,²⁹ they are cumbersome due to the multiple fabrication steps involved. These limitations have fueled the research on flexible nanofabrication methods that can be utilized for high-throughput nanopatterning.^{30–35}

One innovative approach is nanostencil lithography (NSL). NSL is a shadow-mask patterning technique^{36–41} that is widely used in microelectronics and can allow fabrication of structures at sub-100 nm resolution.^{37,39} The method relies on direct deposition of materials through a prepatterned mask. The deposited material could be metallic, dielectric, and organic. The mask, which acts as a stencil, is fabricated on suspended silicon nitride membrane using EBL

* To whom correspondence should be addressed. E-mail: altug@bu.edu.

Received for review: 03/24/2010

Published on Web: 06/18/2010

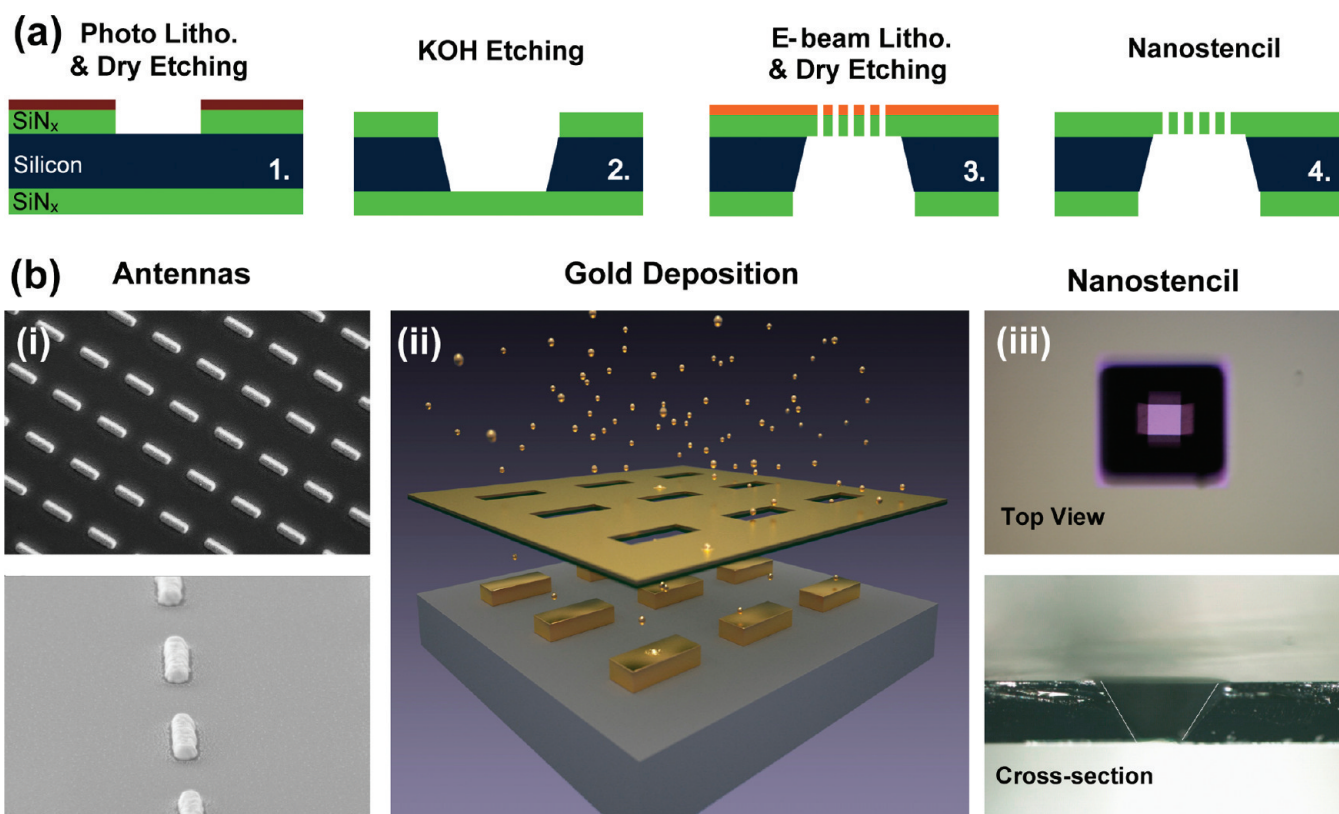


FIGURE 1. Nanostencil lithography, a shadow-mask patterning technique, is used for high-throughput fabrication of plasmonic antenna arrays. (a) Fabrication of free-standing membrane and nanostencil is illustrated from 1 to 4. Dry and wet etching processes and EBL are used for achieving precisely defined pattern of nanoapertures/slits on the membrane. (b) (i) Top and angled SEM images of the gold nanorod with 1100 nm length, 230 nm width, and 100 nm height are shown. (ii) Gold deposition scheme with reusable mask is illustrated. (iii) Top view and cross sectional images of the stencil are shown.

(or FIB) and dry etching methods. The stencils containing large numbers of nanoapertures/nanoslits with variety of shapes, sizes, and arrangements can be fabricated on wafer scale for high throughput nanofabrication applications.³⁹ When placed in contact on a desired substrate, direct deposition of materials (such as noble metal) enables lift-off free fabrication of nanoparticles and nanowires with high reliability and uniformity. Since NSL does not require any resists, it has the advantage of reducing the fabrication steps and allowing the patterning on different types of substrates. Another advantage of NSL is that the masks can be reused to pattern the same nanostructures multiple times with minimal effort.

In this letter, by using nanostencil lithography technique,³⁶ we demonstrate high-throughput fabrication of infrared plasmonic nanorod antenna arrays. Nanorods present a half-wave dipole antenna behavior and support plasmonic resonances linearly scaling with the rod length.⁴² This observation is rather advantageous as it enables tunability of plasmonic resonances over a wide spectral range, from visible wavelengths to the infrared regime.^{16,43} Furthermore, periodic arrangement of the nanorods enables radiative engineering of plasmonic excitations.^{16,44} The antenna arrays can support collective excitations leading to spectrally narrower far-field extinction resonances and far

stronger near-field enhancements than what is achievable with the individual constituent nanoparticles.^{44–46} Here, we show that nanostencil lithography offers the flexibility and the resolution to engineer nanoantenna arrays and can be used to fabricate plasmonic substrates supporting spectrally sharp collective excitations at mid-infrared wavelengths in a high-throughput fashion. Reflection spectra of these antenna arrays are comparable to that of the arrays fabricated by EBL. More importantly, we show that nanostencil masks can be reused multiple times to create series of nanoantenna arrays leading to same optical responses. Our observation is confirmed by optical measurements as well as scanning electron microscopy images. Finally, we demonstrate fabrication of nanostructures in various shapes with a single metal deposition step on different substrates, including nonconducting surfaces (i.e., CaF₂ and glass). This nanofabrication scheme, enabling the reusability of stencil and offering flexibility on the substrate choice and nanopattern design, could significantly speed up the transition of plasmonic devices into the real-world applications.

Nanostencil Lithography for Plasmonic Nanostructure Fabrication. Nanostencil technique, summarized in Figure 1, consists of three stages, (i) fabrication of the free-standing membrane, (ii) patterning on the membrane, and (iii) direct deposition of metallic plasmonic devices. Processing steps

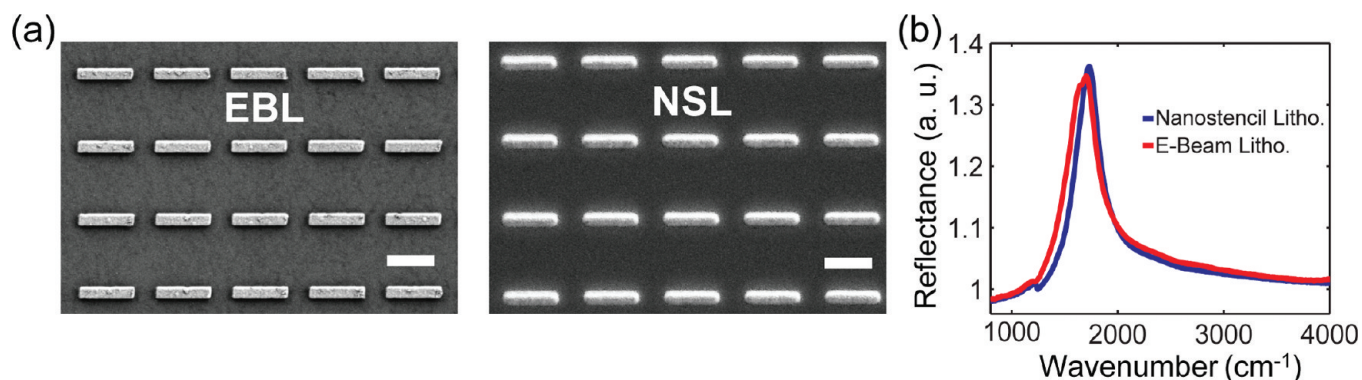


FIGURE 2. Nanostencil lithography is used to fabricate plasmonic nanorod antenna arrays. (a) SEM images of nanorods with 1100 nm length, 230 nm width, and 100 nm height fabricated using EBL (left) and NSL (right) are shown for comparison. White scale bars represent 1 μm . NSL technique for large area patterning of nanorod arrays provides comparable quality with arrays fabricated using EBL. (b) Nanorods fabricated using two different techniques give identical reflection spectrum with resonances at $\sim 1700\text{ cm}^{-1}$.

for free-standing membrane fabrication is illustrated in Figure 1a. An important consideration here is the mechanical strength of the membranes. Highly robust low-pressure chemical vapor deposition (LPCVD) SiN_x films are an excellent choice.^{7,47} We start with 550 μm thick silicon wafer coated with 400 nm thick LPCVD SiN_x on double sides. After cleaning with organic solvents, 2 μm thick MICROPOSIT S1818 positive photoresist is spin coated. Apertures of 800 $\mu\text{m} \times 800\ \mu\text{m}$ on the SiN_x layer are defined by photolithography with SUSS MicroTec MA/BA6Mask Aligner and reactive ion etching (RIE) with Plasma Therm 790 RIE/PECVD System. Then, the chips are immersed in KOH solution to selectively etch Si layer. Finally, $\sim 200\ \mu\text{m} \times 200\ \mu\text{m}$ and 400 nm thick free-standing SiN_x membranes are obtained once the etching stops at the SiN_x layer. Si is etched with 54.7° angle side-wall profile, as shown at Figure 1a.

The second stage is nanoaperture patterning on the membrane. Prior to the patterning, SiN_x layer is thinned down to 70 nm to obtain fully etched nanoapertures. Next steps involve spinning of positive e-beam resist, poly (methylmethacrylate) (PMMA), followed by e-beam exposure using Zeiss Supra 40VP with GEMINI electron-optics column. Here, EBL is needed only once for the creation of the mask, since the mask can be used multiple times. After development of PMMA resist, patterns are transferred to the SiN_x membrane by RIE using SF_6 and Ar gases. The resulting structure used as stencil. The top and the cross sectional views of a fabricated stencil masks are shown in Figure 1b.

The final stage of our nanostencil method involves direct deposition of the plasmonic structures to the desired surface. To get high quality structures, the gap between the substrate and the mask must be minimized.³⁹ The stencil is directly placed on the substrate and secured tightly with clips so that the silicon side is facing up, while the patterned SiN_x layer is nominally kept in contact with the substrate. Here, the sturdiness of the LPCVD SiN_x layer plays important role for the durability of the mask. Directional gold deposition at 3×10^{-6} Torr is performed in CHA-600S e-beam evaporator for 100 nm gold film without depositing any prior adhesion

layer (such as Ti or Cr) (Figure 1b). Unlike EBL, an adhesion layer is not necessary since NSL does not require metal lift-off processes. When the mask is removed from the substrate, it leaves plasmonic nanostructures on the substrate with the shapes complementary to the nanoapertures.

Nanorod Fabrication: Nanostencil versus E-beam Lithography. Using NSL, we successfully fabricated a variety of plasmonic nanostructures, including nanowires and nanoparticles, in different arrangements and on different substrates. In the following, we will particularly focus on the results obtained from the gold nanorod arrays as they act as very efficient infrared plasmonic antennas. Nanorod arrays, obtained by NSL technique, are investigated using SEM and compared against the nanorods with the same dimensions fabricated using EBL. Figure 2a displays two arrays of nanorods (230 nm width and 100 nm height with a periodicity of 1.5 μm) fabricated on silicon substrates using EBL and NSL. No irregularities on the periodicity or the physical dimensions are detected for the nanorod arrays fabricated using NSL. Compared to the dimensions of the corresponding apertures, 15% enlargement is observed in the nanorod lengths and the widths. To obtain nanorods with desired sizes, this enlargement is compensated by scaling the apertures on the stencils. Round edged nanoapertures on the mask caused particles to have rounded tips. Because of the unavoidable gap between the mask and the substrate, scattering of gold particles at 20 nm vicinity of the nanorods has also been observed. As we demonstrate below, however, scattered gold particles have a negligible effect on the optical quality of the structures.

The optical responses of the antennas are the ultimate metrics for determination of the fabricated nanostructure qualities. The reflection spectra are obtained from the NSL fabricated arrays in the mid-IR frequency range and the results are compared with the spectra of the structures fabricated using EBL. Our experimental setup consists of an IR microscope coupled to a Bruker Fourier transform infrared spectrometer with a KBr beam splitter. Light is normally incident on the nanopatterned surface. Reflected infrared

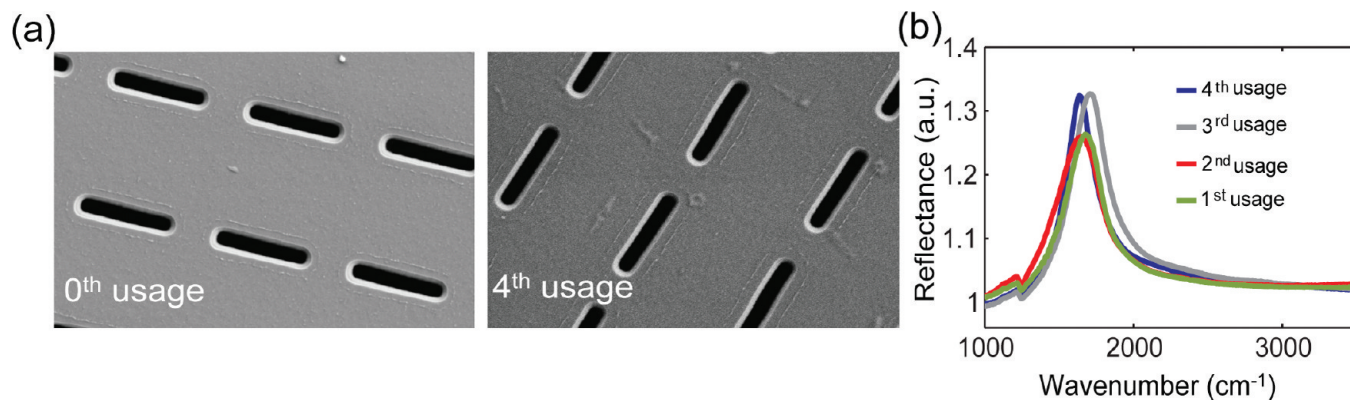


FIGURE 3. Mask can be reused multiple times. (a) SEM images of the same mask are shown before its first usage and after the fourth usage. Apertures have dimensions of 1050 nm length and 200 nm width. No sign of degradation and deformation is observed on the mask after fourth usage. (b) Reflectance spectra are shown for different nanorod arrays obtained from four consecutive depositions using the same mask. The resulting spectra show negligible deviations on resonances (3.5%) around 1700 cm^{-1} .

signal is collected using a Cassagrian reflection optics ($NA = 0.4$) and coupled into a mercury cadmium telluride detector. Reflectance spectrum at Figure 2b shows a strong resonance at the designed wavelength of $5.77 \mu\text{m}$. Absorption losses due to the naturally grown oxide layer on silicon substrates are corrected with baseline fitting. Intensities of the reflected light obtained from the same size arrays are comparable for both fabrication schemes. The spectral line width of the resonances is also comparable to or slightly narrower than that of the arrays fabricated using EBL. These observations indicate plasmonic structures with high optical quality are obtained. We associate the slight narrowing to the absence of an optically lossy adhesion layer (5 nm of Ti), which is normally required in lift-off based nanofabrication schemes for sticking the gold to the substrate. Our spectral and SEM measurements faithfully confirm the feasibility of NSL technique for large area patterning of nanorod antenna arrays with optical qualities achievable by EBL.

Reusability of Stencil for High-Throughput Nanofabrication. The unique advantage of the nanostencil lithography is that stencils can be reused for multiple times. This capability is particularly useful when high-throughput replication of the optimized nanoparticle arrays is desired. After metal deposition, we achieve reuse of the stencils by first dipping them in wet metal etchant and then rinsing in DI water. Here, we used gold etchant to clean the stencil including the remnants inside the nanopertures after deposition. Once the deposited metal is stripped away, the stencil is ready to be used again. SEM images in Figure 3a show the condition of the stencil mask before it is used for the first time and after the fourth usage (and subsequent cleaning). The sizes of the apertures, 1050 and 200 nm in length and width are almost same for both cases. There is no sign of degradation and deformation after the fourth usage. In subsequent usages, we observed that the masks mainly fail due to mechanical cracking. We think thickness of the membrane (only 70 nm) is the main limiting factor for

maximum usage. Increasing the thickness of the membrane should improve the life span of the stencil. Figure 3b shows the reflection spectrum of the four different series of nanorod arrays fabricated on different silicon chips by using the same stencil. The resulting spectra for all the structures have very similar spectral profiles. They show strong resonances around 1700 cm^{-1} with deviations in the spectral peak position less than 3.5%, which could be due to the slight variations in the deposited metal thicknesses and the gap between the mask and the substrate. Our observations clearly indicate that with a single stencil, optimized designs can be replicated many times with a high degree of plasmonic antenna uniformity and similar optical response. This high-throughput fabrication capability is highly advantageous compared to e-beam lithography, which is serial in nature.

Collective Plasmonics and Engineered Plasmonic Nanoantennas by Nanostencil Lithography. As the stencils are fabricated by EBL, NSL preserves the inherent flexibility of EBL in creating wide variety of nanoparticle shapes and composition at high resolution. This ability is especially useful for arrayed structures as interesting physics have been shown in repetitive patterns of dielectric⁴⁸ and metallic (nanoplasmonic)⁴ nanostructures. In the following, we show that periodic arrays of plasmonic nanorods can be radiatively engineered to excite collective plasmons leading to spectrally sharp resonances with extremely strong near fields. Such collective behavior in arrays offers means to boost capabilities of the individual plasmonic nanorods.^{44–46} Collective excitations can be understood from the fundamental principles following the coupled dipole approximation.⁴⁴ Plasmonic nanorods respond to an acting electric field on them with an induced dipole moment, which has maximum strength at the localized plasmon resonance. For an individual antenna, this acting field is simply the electric field of the incident light. Once arrayed, the acting field on an individual antenna includes both (i) the incident field, and

(ii) the sum of the retarded dipolar fields due to the other nanorods in the array¹⁶

$$\begin{aligned}\vec{E}_{\text{acting},i} &= \vec{E}_{\text{incident},i} + \sum_{i \neq j} \vec{E}_{\text{retarded},ij} \\ &= \vec{E}_0 e^{i\vec{k} \cdot \vec{r}_i} + \sum_{i \neq j} (\vec{c}_{ij} \cdot \vec{P}_j) e^{i\vec{k} \cdot \vec{r}_{ij}}\end{aligned}$$

Here, E_0 is the incident field, P_j is the induced polarization of j -th antenna in the array, and c_{ij} is the dipolar interaction matrix among nanorods without the phase term (see Supporting Information in ref 16). Accordingly, the strength of the total field acting on an individual nanorod strongly depends on the phase-delay among the dipolar interactions. This acting field could be extremely large when the scattered fields are almost in-phase for a particular grating order ($\lambda_{\text{incident}} \approx n_{\text{substrate}} d_c / (i^2 + j^2)^{1/2}$). This happens when the diffractive grating order is still evanescent such that the radiative damping of the plasmonic excitations is suppressed. Tuning of the individual antenna resonances (LSPs) to this incident wavelength (where the scattered fields are almost in-phase) strongly enhances the collective behavior^{16,44} and leads to extremely strong near-field excitations that are suitable for applications related to SEIRA, SERS, and second harmonic generation.

For best performances, tailoring of the nanorod arrays requires optimization of the individual nanoantenna characteristics through the rod dimension as well as the phases of the retarded dipolar interactions through the periodicity.⁴⁴ To obtain the individual antenna response, we fabricated randomized (but consistently oriented) arrays of nanorods. The random arrangement of nanorods cancels out any long-range dipolar interactions among the nanorods, while allowing us to measure the individual antenna behavior at high signal-to-noise ratios with an interferometer.^{16,49,50} Figure 4a shows the resonance spectrum of a set of randomized nanorod arrays with varying lengths for a fixed width (230 nm) fabricated on silicon over an area of $100 \times 100 \mu\text{m}^2$. In analogy with half-wave dipole antenna from the microwave theory, nanorod resonances scale linearly with the rod length as $\lambda_{\text{Res}} = 2n_{\text{eff}}L + C$. Here, n_{eff} is the effective refractive index of the surrounding medium (silicon and air) and C accounts for the finite width and height of the antenna. For a cylindrical antenna with hemispherical ends constant C is given by $4Rn_{\text{eff}}/m$,^{42,44,51} where m indicates the order of the resonance ($m = 1$ in our case). As shown in Figure 4b, nanorod resonances closely follow the linear scaling relation. Increasing the rod length results in red shifting of the resonance wavelength. Fitting of the experimentally observed resonance wavelengths to the dipolar antenna formula yields $n_{\text{eff}} = 2.52$. The constant fitting parameter C resulted in an effective cross-sectional radius of 188 nm, which is in close agreement with the average value of the width and the height of the antennas, 170 nm.

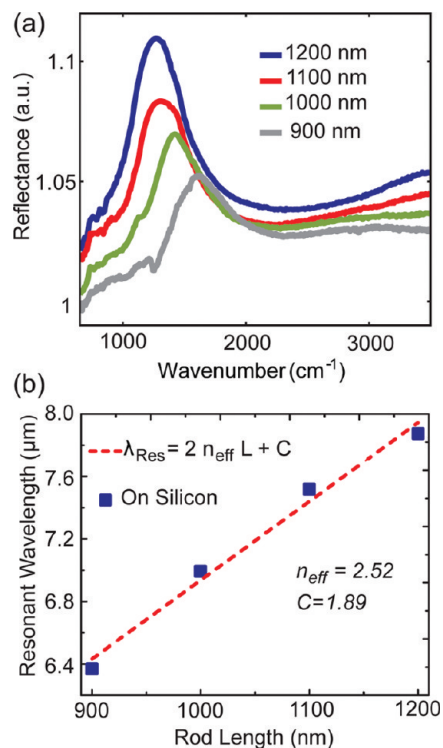


FIGURE 4. Plasmonic gold nanorod arrays fabricated using nano-stencil lithography displays antenna like behavior in Mid-IR frequencies. (a) Reflectance spectra of randomly arranged nanorods with lengths indicated in the legend, 230 nm widths and 100 nm heights. (b) Fundamental ($m = 1$) resonance wavelengths (blue squares) are linearly dependent on the rod length (dashed red line is linear fit). Effective refractive index (n_{eff}) and constant fitting parameter (C) are calculated as 2.52 and 1.89 μm , respectively.

Figure 5a shows spectral narrowing of the far-field responses as a result of collective excitation of the plasmons. The data are shown for nanorod arrays ($L = 1100$ nm) with changing periodicities ($d = 1.5, 1.6, 1.8,$ and $2 \mu\text{m}$). Spectrum of an 1100 nm long individual nanorod antenna indicating LSPR, (obtained from randomized arrays) is also presented for reference (black curve). Slight shifting of the LSP resonance is observed with respect to the ones in reference¹⁶ due to the absence of the titanium layer and the variation of the metal thickness. We also note that periodicity is dominant in controlling the resonance frequencies of the antenna arrays. The effect of the periodicity on the resonance wavelengths and line-widths of the far-field reflectance spectra is summarized in Figure 5b. Here, the dashed line separates the evanescent and the radiative spectral regions for the (1, 0) grating order at the silicon interface for a given periodicity. For periodicities smaller than $d = 1.8 \mu\text{m}$, the diffractive grating order is evanescent and leads to the suppression of the radiative damping. Therefore, significantly narrower far-field spectral response ($\sim 1 \mu\text{m}$ with respect to $\sim 3 \mu\text{m}$ of an individual nanorod) is observed as a result of electromagnetic field confinement within the array. For grating periods $d = 1.8$ and $2.0 \mu\text{m}$, the grating order changes from evanescent to radiative in

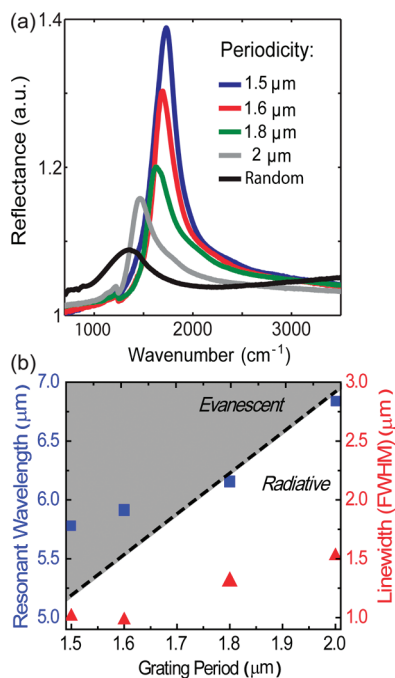


FIGURE 5. Spectral characteristics of periodic nanorod arrays, fabricated using nanostencil lithography are shown. (a) Reflectance spectra of the periodic nanorod antenna arrays with 1100 nm length, 230 nm width, 100 nm height, and periodicities changing from 1.5 to 2 μm (indicated in the legend) are displayed. Spectrum of 1100 nm long individual nanorod antenna (black curve) is also presented for reference. (b) Resonance wavelengths (blue square, left y-axis) and the line widths (red triangles, right y-axis) are shown for varying periodicities. The dashed line separates the evanescent (shaded) and the radiative spectral regions for the first grating order on the silicon/air interface.

nature. Hence, the broadening of the resonances is observed with increased radiative damping.

The spectra shown in Figure 5, including the line widths and the intensities, closely match with the spectra of the nanorod arrays fabricated using EBL. Here, we tuned the

collective resonances of the plasmonic arrays to the amide-I and amide-II vibrational bands of the protein backbone, which are 1660 and 1537 cm⁻¹ respectively. These collective plasmonic excitations accompanied with enhanced near field intensities are highly suitable for ultrasensitive vibrational nanospectroscopy.¹⁶ Further studies on these NSL fabricated antennas for spectroscopic application are currently underway in our research group.

Substrate Flexibility in Nanostencil Lithography. As mentioned above, nanostencil lithography is a resist-free process that allows the transfer of the nanopatterns to any planar substrate whether it is conductive, insulating, or magnetic.³⁶ Such flexibility in substrate choice is in sharp contrast to EBL and FIB lithography, which require conductive substrates or addition of a conducting film.²⁸ Furthermore, resist-based lithography techniques limit the shape and the size of the substrate due to the edge-bead formation during spin coating process. Certain applications may require the usage of nonconductive substrates with irregular shapes. For example, for optical biosensing applications at visible frequencies, either glass or quartz based microscope slides are highly advantageous due to their optical transparency and low cost. Similarly, at mid-IR frequencies, CaF₂ windows are very suitable.⁵² EBL on these insulating substrates requires addition of a conductive film either as a thin ITO layer before the application of EBL resist or as a thin sacrificial metal layer on the e-beam resist. As shown in previous studies, the ITO layer used in the former approach could interfere with the plasmonic responses of metallic nanoparticles,²⁸ while the latter one involves additional fabrication steps. In contrary, using NSL we show here that direct patterning of plasmonic nanoantennas on nonconducting slides can be achieved with a single metal deposition step. The optical responses of gold nanorod arrays fabricated on glass and CaF₂ are shown in Figure 6. The antennas, intentionally distributed randomly, show distinct LSP reso-

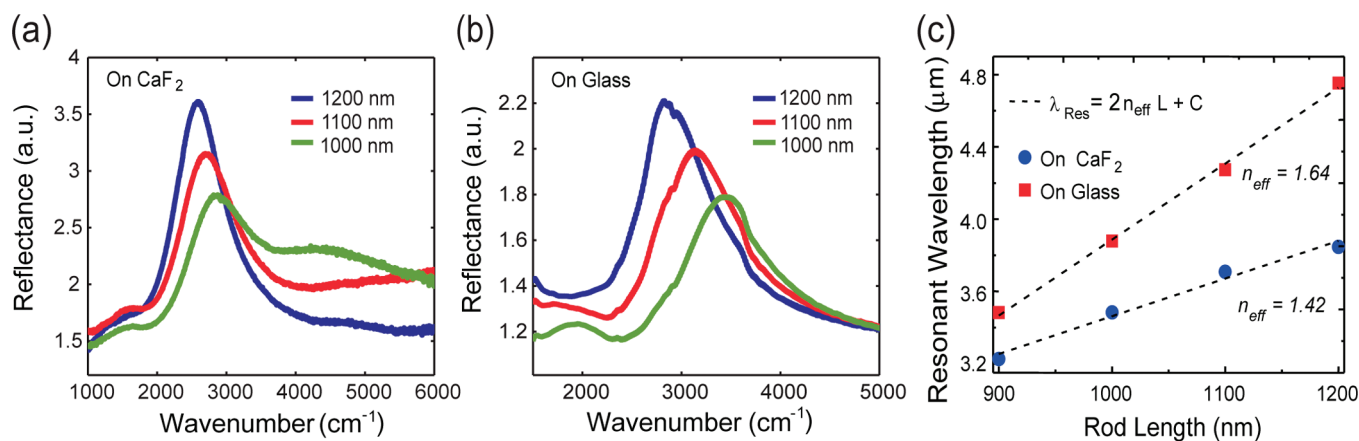


FIGURE 6. Reflectance spectra of randomly distributed nanorods (a) on calcium fluoride and (b) on glass substrate are shown. Legends indicate the rod lengths. CaF₂ substrate supports plasmonic resonances at shorter wavelengths and shows stronger resonances with narrower linewidths compared to the glass. (c) Fundamental ($m = 1$) resonance wavelength on glass (red squares) and on CaF₂ (blue circles) substrates are linearly dependent on the rod length (dashed lines are linear fit). Effective refractive index calculated to be 1.64 for glass and 1.42 for CaF₂ are close to the actual values.

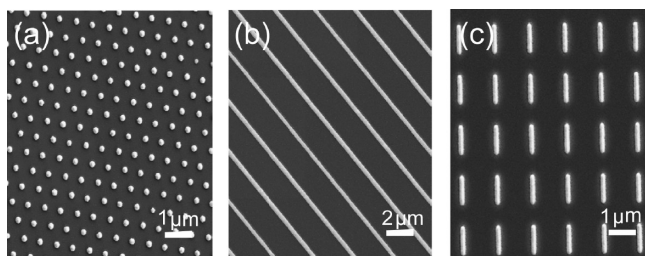


FIGURE 7. Nanostencil lithography allows us to fabricate structures composed of various shapes, dimensions, and materials. SEM images of (a) circular gold nanoantenna arrays with 200 nm diameter and 600 nm period in triangular lattice, (b) gold nanowires with uniform 350 nm width and 50 μm length, (c) gold nanorod arrays are shown. All structures are fabricated on silicon using NSL.

nances. The width and the height of the antennas have been set to 230 and 100 nm, respectively, and the nanorod lengths have been varied from 1000 to 1200 nm. In agreement with the dipole antenna theory, wavelengths of the plasmonic resonances scale linearly with the nanorod length.

For a given nanorod length, the antennas deposited on CaF_2 substrate support plasmonic resonances at shorter wavelengths (longer wavenumbers) with respect to the antennas fabricated on glass surface. This is expected since CaF_2 has a lower refractive index ($n_{\text{CaF}_2} = 1.40$) than glass ($n_{\text{glass}} = 1.51$). Experimentally measured resonances are least-squares fitted to the dipole antenna scaling relation. The estimated refractive index values (1.64 and 1.42 for glass and CaF_2 , respectively) closely match to the actual values. We also observed that antennas fabricated on CaF_2 substrates, compared to the ones on glass, show stronger resonances with narrower line width. This is also expected due to the lower optical absorption of CaF_2 with respect to glass at mid-IR frequencies.

Design Flexibility in Nanostencil Lithography. Given that EBL is used to create stencils for NSL, we inherently preserve the flexibility and the accuracy of EBL in creating plasmonic nanostructures in variety of shapes and designs. This can be achieved by simply changing the aperture pattern on the silicon nitride membrane. Figure 7a shows SEM images of circular gold nanoantenna arrays fabricated in triangular lattice on silicon substrate. The particles have 200 nm diameter with 600 nm periodicity. The diameters of the nanoparticles are 30 nm larger than the corresponding circular nanoapertures. The shape, size and periodicity distribution of these smaller nanoparticles have been observed to be very uniform over the area of the stencil (100 μm \times 100 μm). As the dimensions of the particle reduce, the resonances shift toward the visible wavelength regime. High-throughput fabrication of plasmonic substrates supporting resonances at visible spectrum could be important for nonlinear photonic and photovoltaic applications.⁵³ Figure 7b shows SEM images of Au nanowires with 350 nm width and 50 μm length fabricated on silicon over 50 \times 50 μm area. The corresponding nanoslits were 300 nm and 50 μm in width and

length. No discontinuity or width fluctuation is observed on the wires. The wires fabricated by the stencil technique can carry electrical signals.⁵⁹ In addition, these wires can also be used optically as on-chip plasmonic waveguides for ultradense optical interconnects.²⁵

Conclusion. In this work, using nanostencil lithography,^{36–41} we have demonstrated a novel strategy for high-throughput nanofabrication of engineered plasmonic devices. This technique allows fabrication of nanoplasmonic devices with high uniformity and repeatability without using operationally slow and expensive electron/ion-beam lithography tools. Fabricated structures are characterized by scanning electron microscopy and optical measurements. Devices, fabricated using NSL technique are shown to have comparable optical characteristics with respect to the arrays fabricated by EBL. We show that the stencil can be reused for high-throughput fabrication of antenna arrays by simply removing the metal residue with a mild metal etchant. We also show that NSL offers the flexibility and the resolution to radiatively engineer nanoantenna arrays for excitation of collective plasmonic resonances. These excitations, by enabling spectrally narrow far-field resonances and enhanced near-field intensities, are highly suitable for ultrasensitive vibrational nanospectroscopy. In addition to its high-throughput capability, NSL enables fabrication of plasmonic devices on surfaces otherwise difficult to work with electron/ion beam techniques. Here, we have demonstrated successful fabrication of plasmonic devices on nonconducting surfaces such as glass and CaF_2 . As proof of the versatility of the NSL technique, variety of plasmonic structures such as nanowires and nanodisk are also fabricated. We believe that NSL can facilitate a significant progress toward the wide usage of nanoplasmonic devices.

Acknowledgment. We would like to acknowledge Shyam Erramilli. This work is supported in part by NSF CAREER Award (ECCS-0954790), ONR Young Investigator Award, Massachusetts Life Science Center New Investigator Award, NSF Engineering Research Center on Smart Lighting (EEC-0812056), Boston University Photonics Center, and Army Research Laboratory.

REFERENCES AND NOTES

- (1) Ozbay, E. *Science* **2006**, *311*, 189–193.
- (2) Maier, S. *Plasmonics: Fundamentals and Applications*; Springer: New York, 2007.
- (3) Zia, R.; Schuller, J. A.; Brongersma, M. L. *Mater. Today* **2006**, *9*, 20–27.
- (4) Barnes, W. L.; Dereux, A.; Ebbesen, T. W. *Nature* **2003**, *424*, 824–830.
- (5) Lal, S.; Link, S.; Halas, N. J. *Nat. Photonics* **2007**, *1*, 641–648.
- (6) Artar, A.; Yanik, A. A.; Altug, H. *Appl. Phys. Lett.* **2009**, *95*, No. 051105.
- (7) Yanik, A. A.; Huang, M.; Artar, A.; Chang, T. Y.; Altug, H. *Appl. Phys. Lett.* **2010**, *96*, No. 021101.
- (8) Kinkhabwala, A.; Yu, Z.; Fan, S.; Avlasevich, Y.; Mullen, K.; Moerner, W. E. *Nat. Photonics* **2009**, *3*, 654–657.
- (9) Levene, M. J.; Korlach, J. S.; Turner, W.; Foquet, M.; Craighead, H. G.; Webb, H. G. *Science* **2003**, *299*, 682–686.

- (10) Kneipp, K.; Wang, Y.; Kneipp, H.; Perelman, L. T.; Itzkan, I.; Dasari, R. R.; Feld, M. S. *Phys. Rev. Lett.* **1997**, *78*, 1667–1670.
- (11) Lal, S.; Grady, N. K.; Goodrich, G. P.; Halas, N. J. *Nano Lett.* **2006**, *6*, 2338–2343.
- (12) McFarland, A. D.; Young, M. A.; Dieringer, J. A.; Van Duyne, R. P. *J. Phys. Chem. B* **2005**, *109*, 11279–11285.
- (13) Shamsaiea, A.; Heima, J.; Yanik, A. A.; Irudayaraj, J. *Chem. Phys. Lett.* **2008**, *461*, 131–135.
- (14) Cubukcu, E.; Zhang, S.; Park, Y.-S.; Bartal, G.; Zhang, X. *Appl. Phys. Lett.* **2009**, *95*, No. 043113.
- (15) Kim, S.; Jin, J.; Kim, Y.-J.; Park, I.-Y.; Kim, Y.; Kim, S.-W. *Nature* **2008**, *453*, 757–760.
- (16) Adato, R.; Yanik, A. A.; Amsden, J. J.; Kaplan, D. L.; Omenetto, F. G.; Hong, M. K.; Erramilli, S.; Altug, H. *Proc. Natl. Acad. Sci. U.S.A.* **2009**, *106* (46), 19227–19232.
- (17) Oulton, R. P.; Sorger, V. J.; Zentgraf, T.; Ma, R. M.; Gladden, C.; Dai, L.; Bartal, G.; Zhang, X. *Nature* **2009**, *461*, 629–632.
- (18) Noginov, M. A.; Zhu, G.; Belgrave, A. M.; Bakker, R.; Shalaev, V. M.; Narimanov, E. E.; Stout, S.; Herz, E.; Suteewong, T.; Wiesner, U. *Nature* **2009**, *460*, 1110.
- (19) Falk, A. L.; Koppens, F. H. L.; Yu, C.; Kang, K.; de Leon Snapp, N. P.; Akimov, A. V.; Jo, A. V.; Lukin, M. D.; Park, H. *Nat. Phys.* **2009**, *5*, 475–479.
- (20) Taubner, T.; Korobkin, D.; Urzhumov, Y.; Shvets, G.; Hillenbrand, R. *Science* **2006**, *313*, 5793–1595.
- (21) Fang, N.; Lee, H.; Sun, C.; Zhang, X. *Science* **2005**, *308* (5721), 534–537.
- (22) Smith, D. R.; Pendry, J. B.; Wiltshire, M. C. K. *Science* **2004**, *305*, 788–792.
- (23) Shalaev, V. M.; Cai, W.; Chettiar, U. K.; Yuan, H. K.; Sarychev, A. K.; Drachev, V. P.; Kildishev, A. V. *Opt. Lett.* **2005**, *30*, 24–3356.
- (24) Chen, H. T.; Padilla, W. J.; Cich, M. J.; Azad, A. K.; Averitt, R. D.; Taylor, A. J. *Nat. Photonics* **2009**, *3*, 148.
- (25) MacDonald, K. F.; Sa’msen, Z. L.; Stockman, M. I.; Zheludev, N. I. *Nat. Photonics* **2009**, *3*, 55.
- (26) Brewer, G. R. *Electron beam technology in microelectronic fabrication*; Academic Press: New York, 1980.
- (27) Melngailis, J. *J. Vac. Sci. Technol., B* **1987**, *5* (2), 469–495.
- (28) Auguié, B.; Barnes, W. L. *Phys. Rev. Lett.* **2008**, *101*, 143902.
- (29) Sun, X.; Zhuang, L.; Zhang, W.; Chou, S. Y. *J. Vac. Sci. Technol., B* **1998**, *16* (6), 3922–3925.
- (30) Solak, H. H.; Ekinci, Y. *J. Vac. Sci. Technol., B* **200725**, (6), 2123–2126.
- (31) Henzie, J.; Lee, J.; Lee, M. H.; Hasan, W.; Odom, T. W. *Annu. Rev. Phys. Chem.* **2009**, *60*, 147–165.
- (32) Boltasseva, A. *J. Opt. A: Pure Appl. Opt.* **2009**, *11*, 114001.
- (33) Aksu, S.; Altug, H. *Mater. Res. Soc. Symp. Proc.* **2010**, 1208E.
- (34) Haynes, C. L.; Van Duyne, R. P. *J. Phys. Chem. B* **2001**, *105*, 5599–5611.
- (35) Prikulis, J.; Hanarp, P.; Olofsson, L.; Sutherland, D.; Kall, M. *Nano Lett.* **2004**, *4*, 1003–1007.
- (36) Burger, G. J.; Smuldersa, E. J. T.; Berenschota, J. W.; Lammerinka, T. S. J.; Fluitmana, J. H. J.; Imaib, S. *Sens. Actuators, A* **1996**, *54* (1–3), 669–673.
- (37) Yan, X.-M.; Contreras, A. M.; Koebel, M. M.; Liddle, J. A.; Somorjai, G. A. *Nano Lett.* **2005**, *5* (6), 1129–1134.
- (38) Gross, L.; Schlittler, R. R.; Meyer, G.; Vanhaverbeke, A.; Allenspach, R. *Appl. Phys. Lett.* **2007**, *90*, No. 093121.
- (39) Vazquez-Mena, O.; Villanueva, G.; Savu, V.; Sidler, K.; van den Boogaart, M. A. F.; Brugger, J. *Nano Lett.* **2008**, *8* (11), 3675–3682.
- (40) Selvarasah, S.; Chao, S. H.; Chen, C.-L.; Sridhar, S.; Busnaina, A.; Khademhosseini, A.; Dokmeci, M. R. *Sens. Actuators A* **2008**, *145*, 306–315.
- (41) Champagne, A. R.; Couture, A. J.; Kueemmeth, F.; Ralph, D. C. *Appl. Phys. Lett.* **2003**, *82*, 1111.
- (42) Novotny, L. *Phys. Rev. Lett.* **2007**, *98*, 266802.
- (43) Lee, K.-S.; El-Sayed, M. A. *J. Phys. Chem. B* **2006**, *110*, 19220–19225.
- (44) Adato, R.; Yanik, A. A.; Wu, C. H.; Shvets, G.; Altug, H. *Opt. Express* **2010**, *18* (5), 4526–4537.
- (45) Zou, S.; Schatz, G. C. *Nanotechnology* **2006**, *17*, 2813–2820.
- (46) Lamprecht, B.; Schider, G.; Lechner, R.; Ditlbacher, H.; Krenn, J.; Leitner, A.; Aussenegg, F. *Phys. Rev. Lett.* **2000**, *84*, 4721.
- (47) Huang, M.; Yanik, A. A.; Chang, T. Y.; Altug, H. *Opt. Express* **2009**, *17* (26), 24224–24233.
- (48) Altug, H.; Englund, D.; Vuckovic, J. *Nat. Phys.* **2006**, *2*, 484–487.
- (49) Yanik, A. A.; Adato, R.; Erramilli, S.; Altug, H. *Opt. Express* **2009**, *17* (23), 20900–20910.
- (50) Yanik, A. A.; Wang, X.; Erramilli, S.; Hong, M. K.; Altug, H. *Appl. Phys. Lett.* **2008**, *93*, No. 081104.
- (51) Cubukcu, E.; Capasso, F. *Appl. Phys. Lett.* **2009**, *95*, 201101.
- (52) Harris, D. C. *Materials for infrared windows and domes: properties and performance*; SPIE: Bellingham, WA, 1999.
- (53) Atwater, H. A.; Polman, A. *Nat. Mater.* **2010**, *9*, 205–213.